Journal of Alloys and Compounds 582 (2014) 603–608

Contents lists available at ScienceDirect

Journal of Alloys and Compounds

journal homepage: www.elsevier.com/locate/jalcom

Morphology controllable and highly luminescent monoclinic $LaPO_4:Eu^{3+}$ microspheres

Mei Yang [a], Hongpeng You [b], Youlong Liang [a], Jingzhou Xu [a], Fan Lu [a], Liming Dai [a,c,*], Yong Liu [a,*]

[a] Institute of Advanced Materials for Nano-Bio Applications, School of Ophthalmology & Optometry, Wenzhou Medical University, Wenzhou, Zhejiang 325027, China
[b] State Key Laboratory of Rare Earth Resource Utilization, Changchun Institute of Applied Chemistry Chinese Academy of Sciences, Changchun, Jilin 130022, China
[c] Center of Advanced Science and Engineering for Carbon (Case4Carbon), Department of Macromolecular Science and Engineering, Case Western Reserve University, Cleveland, OH 44106, United States

ARTICLE INFO

Article history:
Received 14 May 2013
Received in revised form 8 August 2013
Accepted 13 August 2013
Available online 23 August 2013

Keywords:
Controllable morphology
Highly luminescence
$LaPO_4:Eu^{3+}$ microspheres

ABSTRACT

A facile, but effective, two-step method was developed to prepare monoclinic $LaPO_4:Eu^{3+}$ microspheres composed of microprisms with a controllable morphology. XRD and SEM studies revealed a spherical morphology and crystalline structure for the resulting material. It was also found that $LaPO_4:Eu^{3+}$ microspheres prepared at 800 °C showed a higher luminescent intensity than primary hexagonal $LaPO_4:Eu^{3+}$ microprisms. Furthermore, the luminescent performance of $LaPO_4:Eu^{3+}$ microspheres was demonstrated to reach the standards of the $LaPO_4:Eu^{3+}$ bulk material under the same conditions. These results suggest possibilities for the use of as-synthesized monoclinic $LaPO_4:Eu^{3+}$ microspheres as alternatives to replace intrinsically uneven bulk materials for many application areas, including light display systems and optoelectronic devices.

1. Introduction

Lanthanide orthophosphate ($LnPO_4$) and lanthanide (III)-doped lanthanide orthophosphate ($LnPO_4:Ln^{3+}$) have attracted much attention due to their unique photo-luminescent properties and various potential applications in various areas, including color displays [1], light sources [2,3], field-effect transistors [4], solar cells [5], and biomedical labels [6]. Recently, photo-luminescent properties and related energy transference of $Na_3–Gd_{1-x}Eu_x(PO_4)_2$ phosphors has been demonstrated by Ju and co-workers [2]. To further enhance the photoluminescence of $GdPO_4:Tb^{3+}$ phosphors under UV excitation, many efforts such as incorporation of ZnO and modification of annealing temperatures have been reported [3]. Although bulk materials of $LnPO_4$ and $LnPO_4:Ln^{3+}$ are useful because of their good luminescent intensity, their practical applications of bulk materials are still limited by their uneven sizes and/or some of their uncontrollable properties. This is because the light excitation cannot reach the center of the phosphor if its size is too big and much of the phosphor material is wasted. If the size of the phosphor is far away from the wavelength of the exciting light, however, the exciting light energy may be wasted [7,8]. Therefore, it is essential for the size of phosphor to be matched with the exciting light source for a highest luminescent efficiency. Thus it is a big challenge to control the size of phosphor bulk materials for practical applications. In this work, we present our recent efforts on the preparation of $LnPO_4$ and $LnPO_4:Ln^{3+}$ microspheres with controllable sizes and enhanced photoluminescent properties.

More recently, nano/micro-scaled $LnPO_4$ materials have been synthesized by various methods. For example, zero-dimensional (0D) $LaPO_4:Ln^{3+}$ (e.g. Eu, Ce, Tb) nanocrystals have been prepared using a facile solvothermal process [9]. One-dimensional (1D) GdPO4 nanorods have also been developed via a hydrothermal method [10]. In our previous work, we have synthesized $LaPO_4:Ln^{3+}$ (e.g. Ce, Tb) core/shell nanowires through a direct precipitation in a water-based system [11]. However, there is still a challenge for fabrication of multidimensional $LaPO_4$ structures with self-assembled hierarchical architectures [12]. Hierarchical self-assemblies with unique morphologies are attractive building blocks for various functional materials with novel properties [13]. In this regard, we employed a simple but effective, two-step method for controllable growth of bundles of hexagonal $LaPO_4:Eu^{3+}$ microprisms and their microspheric self-assemblies, followed by subsequent annealing at different temperatures in air to produce monoclinic $LaPO_4$ in this work. The thermal annealing changed the crystal structure and increased the luminescent intensity of the product significantly, as discussed later. Indeed, the luminescent performance of annealed $LaPO_4:Eu^{3+}$ microspheres reached the standards of $LaPO_4:Eu^{3+}$ bulk materials. These unique proper-

* Corresponding authors. Address: Institute of Advanced Materials for Nano-Bio Applications, School of Ophthalmology & Optometry, Wenzhou Medical University, Wenzhou, Zhejiang 325027, China. Tel.: +86 57788067973 (Y. Liu).
E-mail addresses: liming.dai@case.edu (L. Dai), yongliu1980@hotmail.com (Y. Liu).

0925-8388/$ - see front matter © 2013 Elsevier B.V. All rights reserved.
http://dx.doi.org/10.1016/j.jallcom.2013.08.091

ties of the resulting monoclinic $LaPO_4$ microspheres suggest their potential applications as a substitute of bulk countparts for many applications, such as optical displays and other optoelectronic devices. Furthermore, the newly-developed two-step preparation method provides new possibilities for the preparation of other functional materials with similar hierarchical structures.

2. Experimental procedures

2.1. Materials and reagents

La_2O_3 (99.999%), Eu_2O_3 (99.999%), were purchased from Wuxi Yiteng Rare-Earth Limited Corporation. Citric acid monohydrate ($C_6H_8O_7{\cdot}H_2O$), cetyltrimethylammonium bromide (CTAB), and $(NH_4)_2HPO_4$ were provided by Beijing Chemical Corporation. All reagents were analytical grade and used as received without further purification.

2.2. Synthesis of $La_{0.95}Eu_{0.05}$ $(NO_3)_3{\cdot}6H_2O$

$La_{0.95}Eu_{0.05}(NO_3)_3{\cdot}6H_2O$ were obtained by dissolving La_2O_3 (15.46 g) and Eu_2O_3 (0.88 g) in a dilute aqueous solution of HNO_3 (0.5 mg/mL) with an exact stoichiometry shown in the molecular formula under heating with agitation, followed by solvent evaporation.

2.3. Synthesis of $LaPO_4$:Eu^{3+} microspheres and bulk materials

In a typical experiment, 2 mmol $La_{0.95}Eu_{0.05}(NO_3)_3{\cdot}6H_2O$ and 3 mmol citric acid were dissolved in deionized water, followed by addition of 20 mL ethanol–water solution (v/v = 4:1) containing 3 mmol CTAB and 3 mmol $(NH_4)_2HPO_4$. Transparent solution was obtained when 3–4 mL HNO_3 (1.4 mg/mL) was introduced. The resulting solution was subsequently transferred into a Teflon-lined autoclave, maintaining at 90 °C for 10 h. After cooling down to room temperature with air naturally, precipitate was formed, collected, and washed with deionized water and ethanol several times prior to drying in air at 60 °C for 12 h. The monoclinic phase $LaPO_4$ was consequently obtained after annealing samples at different temperatures over 500–800 °C for 2 h in air atmosphere. For comparison, the bulk material of $LaPO_4$:Eu^{3+} was prepared according to the method reported by Hashimoto and co-workers [14] (see Supplementary Materials for the detailed synthesis process).

2.4. Characterization

The morphology of the final product was examined using a field emission scanning electron microscope (FESEM) (HITACHI S-4800). TEM image and selected area electron diffraction pattern (SAED) were obtained using a JEOL JEM 2010 Transmission Electron Microscope (TEM) operating at an accelerating voltage of 200 kV. XRD patterns were measured by a Rigaku-D X-ray powder Diffractometer with Cu K radiation (λ = 1.54 Å). TG/DTA measurements were performed on a Pyris Diamond TG/DTA with the heating rate of 10 °C min^{-1} from 40 °C to 800 °C. Fourier transform infrared spectroscopic (FT-IR) measurements were carried out on BRUKER Vertex 70 FTIR using KBr pellets. Excitation and emission spectra were determined by a Hitachi F-4500 fluorescence spectrophotometer equipped with a 150 W xenon lamp as the excitation source. The luminescence decay curves were carried out with a Lecroy Wave Runner 6100 digital oscilloscope (1 GHz) using a tunable laser (pulse width = 4 ns, gate = 50 ns) as the excitation source (Continuum Sunlite OPO). All measurements were performed at room temperature unless otherwise stated.

3. Results and discussion

SEM images were taken at various temperatures for the morphology study. As shown in Fig. 1(a) and (b), the sample prepared at 90 °C shows a spherical hierarchical architecture composed of irregular microprisms. The diameter of microspheres is to be about 5–8 μm while the diameter of the densely-packed prisms is around 1 μm. These spherical self-assemblies are very stable even after being annealed at 800 °C, which caused only a little change in the size of microspheres (Fig. 1(c) and (d)).

The sample obtained at 90 °C for 2 h was selected for characterization by TEM and the corresponding selected area electron diffraction pattern measurements (SAED). As can be seen in Fig. 2(a), a spheric assemble with all microrods grown out from the same center was observed in consistence with the SEM examination. Fig. 2(b) is the SAED pattern taken from one prism within microspheres. Indexes of crystal faces were calculated and results

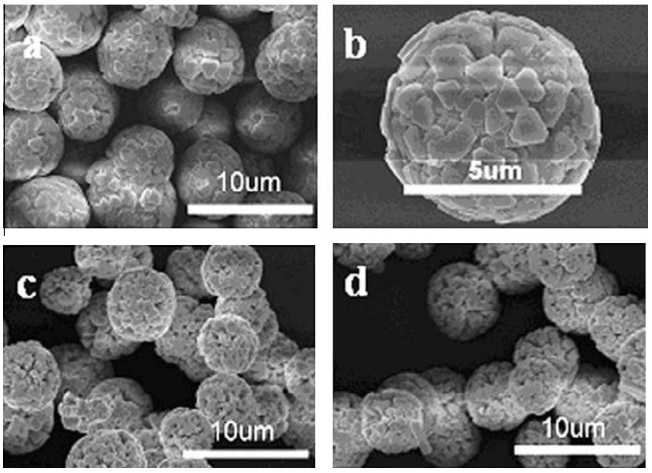

Fig. 1. SEM images of (a) $LaPO_4$:Eu^{3+} microspheres obtained at 90 °C for 10 h, (b) higher resolution of (a), followed by annealing at (c) 500 °C, and (d) 800 °C for 2 h, respectively.

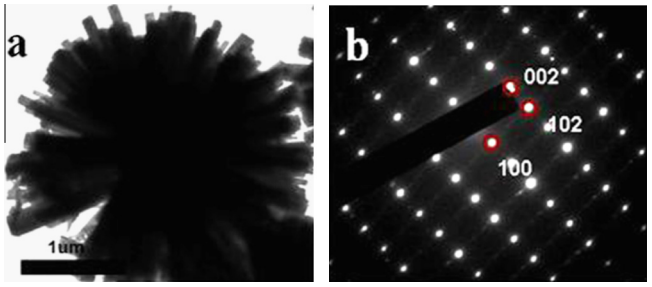

Fig. 2. (a) The TEM image of the as-synthesized product obtained at 90 °C for 2 h and (b) the selected area electron diffraction pattern.

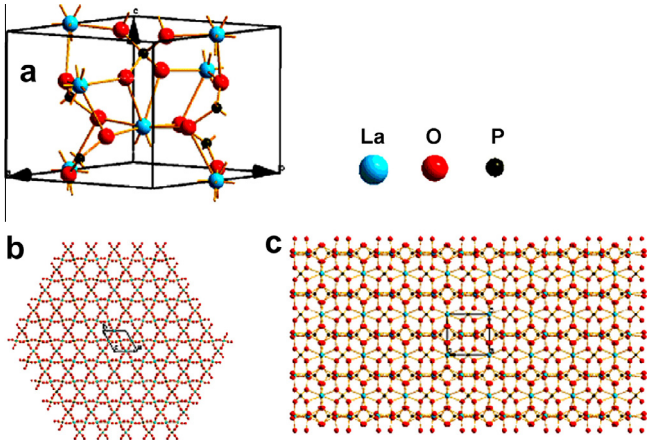

Fig. 3. Simulated crystal structures of $LaPO_4$. (a) the crystal structure, (b) packing view along the c axis, and (c) packing view along the *a* axis.

are indicated in the insert of Fig. 2(b), which, together with corresponding XRD patterns (Fig. 5(a)), confirm a single crystalline nature of the prism.

The observed formation of one-dimensional prisms can be attributed to the inner cell structure of the hexagonal $LaPO_4$, while the simulated crystal structure of $LaPO_4$ is shown in Fig. 3. The overall structure of the hexagonal $LaPO_4$ can be seen as columns containing alternate lanthanum and phosphate ions, extending along the *c*-axis. Each column is linked to four neighboring columns (Fig. 3(b)). The packing structure of the hexagonal $LaPO_4$

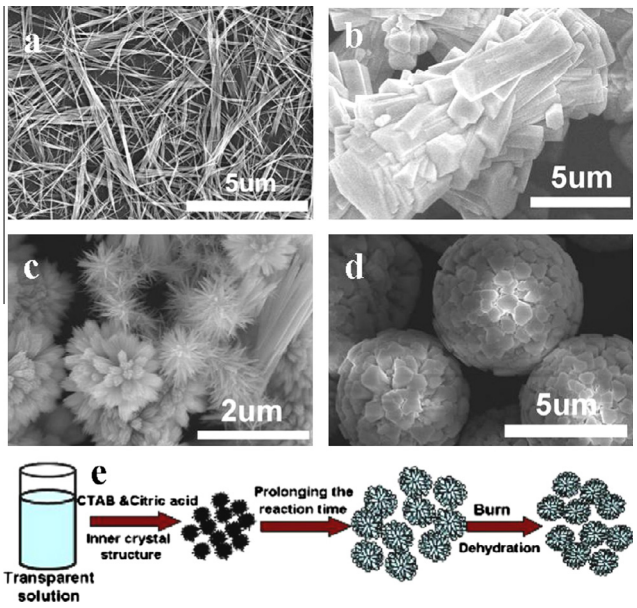

Fig. 4. SEM images of products obtained under different conditions. (a) 3 mmol CTAB, 0 mmol citric acid, (b) 3 mmol citric acid, 0 mmol CTAB, (c) 90 °C, 2 h, (d) 90 °C, 10 h, and (e) as the schematic formation of microspheres.

viewing along the *a*-axis can be described as an infinite linear chain, parallel to the *c*-axis (Fig. 3(c)). This 1D characteristic of hexagonal $LaPO_4$ should play crucial roles in determining final one-dimensional prisms [4].

The formation process of the microsphere was further investigated and schematically shown in Fig. 4(e). Along the 1D characteristic of the hexagonally structured $LaPO_4$, the presence of CTAB is necessary for the controlled formation of the one-dimensional prism as CTAB is a soft template that can facilitate the growth of the 1D structure [15–17]. Upon addition of CTAB into the reaction solution, resultant CTA^+ ions could adsorb on the surface of the nuclei and serve as the growth controller and agglomeration inhibitor [17]. Nanorods were observed (Fig. 4(a)) by adding only CTAB without citric acid under the same condition. When only citric acid was introduced into the reaction system without CTAB, however, the resulting morphology revealed that a hexagonal prism in the middle and many small uncompleted prisms tightly grew on the sides (Fig. 4(b)). Functional groups, such as carboxylic acid and hydroxyl groups, in the citric acid are useful for chelating and selectively binding to specific crystallographic facets. During a typical synthesis process, citric acid firstly reacted with La^{3+} ions to form citrate complexes. The ion-exchange reaction between PO_4^{3-} and citrate ions would then occur after the addition of the phosphorus source, leading to the formation of $LaPO_4$ under hydrothermal conditions. Reaction velocity might be regulated by the release speed of the complex. In addition, the special molecular structure of citric acid may facilitate its selective binding to sideways of pre-formed prisms [18,19], resulting in further aggregation of the newly formed nuclei on pre-formed prisms and subsequent formation of final microspheres. As a result, the nuclei of the product was found to be flower-like microspheres consisting of nanorods (Fig. 4(c)). Due to synergistic effects from both CTAB and citric acid on the inner crystal structure, the morphology of the nuclei gradually changed to hexagonal $LaPO_4$ microspheres containing microprisms after long-time reaction (e.g. 10 h), (Figs. S1a, S1b and Fig. 4(d)). Following the annealing process, both residual reagents (such as CTAB and citric acid) and water (either from the surface or in the crystal structure of resulting materials) would be burned rapidly at the high temperature (confirmed by TGA/DTA results shown in Fig. 5(b)), resulting in the formation of microspheres with final sizes.

XRD patterns of $LaPO_4:Eu^{3+}$ microspheres obtained at 90 °C for 10 h, followed by annealing at different temperatures for 2 h, are

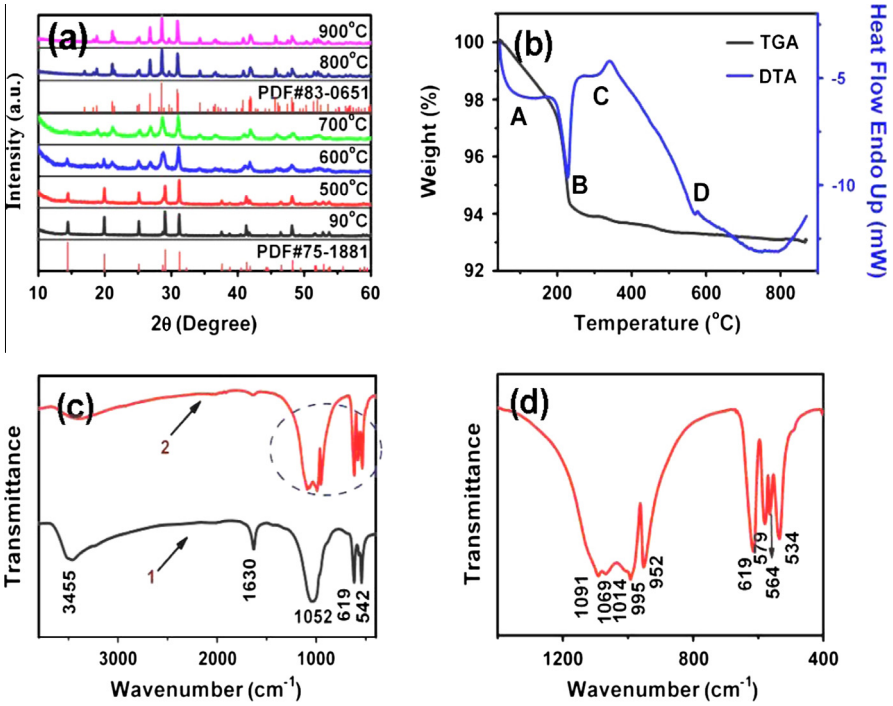

Fig. 5. (a) XRD patterns of $LaPO_4:Eu^{3+}$ microspheres obtained at 90 °C for 10 h, followed by annealing at different temperatures for 2 h, (b) TGA/DTA curves of $LaPO_4:Eu^{3+}$ microspheres obtained at 90 °C for 10 h, (c) FT-IR spectra of the hexagonal $LaPO_4$ (Curve 1) compared to the monoclinic $LaPO_4$ (Curve 2), and (d) the enlarge spectrum of the circled part in Curve 2 of (c).

shown in Fig. 5(a). Based on XRD results, it is worth to point out that the annealing temperature plays an important role in regulating resultant crystalline structures. Phase structures of materials obtained by annealing below 500 °C remain hexagonal $LaPO_4$ (JCPDS 46-1439) with no additional peak for any other phase (black and red curves, Fig. 5(a)). When the annealing temperature increased to 600 °C, character peaks of monoclinic $LaPO_4$ were observed at 18.9°, 21.1°, 26.8° and 34.3° in the corresponding XRD profile (blue curve, Fig. 5(a)). When the annealing temperature was further increased to 800 °C, all diffraction peaks represented by JCPDS 32-0493 appeared, suggesting that a pure monoclinic phase of $LaPO_4$ formed (dark blue curve, Fig. 5(a)). The phase structure remained to be monoclinic $LaPO_4$ for the sample being annealed even at 900 °C (pink curve, Fig. 5(a)). These results clearly demonstrate that phase structures of $LaPO_4$ can be controlled by annealing temperatures. The hexagonal phase formed at low-temperatures can be readily converted into the stable monoclinic structure with increasing annealing temperatures to compensate the free energy difference between the hexagonal and monoclinic phases. Furthermore, we found that the peak width increased with increasing the annealing temperature, especially after the formation of the monoclinic $LaPO_4$ at the annealing temperature above 600 °C. Thus, the phase structure transition from the hexagonal to monoclinic, caused the size reduction for the newly formed monoclinic phase crystal cell, and broadened peaks in XRD patterns.

In order to further confirm influence of the temperature on the phase conversion, we have performed TGA/DTA measurements. As shown in Fig. 5(b), two main distinguished weight loss processes were observed for the as-synthesized hexagonal $LaPO_4$. The first weight loss below 130 °C is due to the release of water molecules adsorbed on the product, which shows a weak endothermic peak centered at 100 °C in the DTA curve (Peak A of the blue profile in Fig. 5(b)). The other widespread weight loss over 130–500 °C can be attributed to the progressive dehydration of the hexagonal phase (130–350 °C) as well as the burn-off of remained organic reagents (350–500 °C, a small weight loss process). Two endothermic peaks located at around 180 and 340 °C (Peak B and C) are seen in the corresponding DTA curve. The hydration ratio of the resulting $LaPO_4$ can be roughly calculated from the weight loss in the range of 130 and 350 °C, which indicates the presence of $LaPO_4{\cdot}0.5H_2O$. Additionally, the exothermic peak around 600 °C in the DTA curve (Peak D) is arising from the phase transition in the product. The TG/DTA results are well consistent with corresponding XRD measurements.

The as-mentioned phase transition is further confirmed by FT-IR spectra for the hexagonal $LaPO_4$ (Curve 1, Fig. 5(c)) and monoclinic (Curve 2, Fig. 5(c)) $LaPO_4$. Two bands at 1630 and 3455 cm^{-1} observed at both samples can be attributed to the hydration water (O–H bond) in as-prepared powders. The other bands presented are attributed to phosphate groups. In particular, the band at 1052 cm^{-1} in the hexagonal phase of $LaPO_4$ arises from a characteristic asymmetry stretch vibration of PO_4^{3-} groups (Curve 1, Fig. 5(c)), while bands at 619 and 542 cm^{-1} are related to the bend vibration of O–P–O [20]. Five characteristic bands at 1093, 1060, 1024, 993, and 954 cm^{-1} were observed in the FI-IR spectrum of the monoclinic phase of $LaPO_4$ (Curve 2, Fig. 5(c) and (d)), which are associated with the bend of P–O of PO_4^{3-} groups. Four bands at 541, 564, 579, and 617 cm^{-1} are due to the asymmetry stretch vibration of O–P–O of PO_4^{3-} groups in the monoclinic $LaPO_4$ [21]. Compared to the spectrum of the hexagonal $LaPO_4$, more FT-IR bands were found at the monoclinic $LaPO_4$, which could be attributed to a phase-transition-induced change in the coordinate number of La atoms from 8-fold coordination in hexagonal $LaPO_4$ to 9-fold coordination in monoclinic $LaPO_4$. Possible structural distortion of tetrahedral phosphate groups in the monoclinic $LaPO_4$ led to a further increase in numbers of FT-IP bands (Curve 2 Fig. 5(c) and (d)).

We further studied excitation and emission behaviors of $LaPO_4$ microspheres prepared at 90 °C and annealed at different temperatures. The excitation spectra (Fig. 6(a)) exhibit a broad band centered at 260 nm related to the charge transfer (CT) from the 2p orbital of the O^{2-} ions to the 4f orbital of Eu^{3+} ions. Other minor peaks at 322, 363, 385, 396, and 468 nm are associated with the direct excitation of electrons for the f–f shell transitions in Eu^{3+} ions. It was also found in Fig. 6(a) that the CT transition band over 200–300 nm redshifted with increasing annealing temperatures. The CT band position in the excitation spectra is usually constant for a particular crystal structure, but it varies as a function of host lattice parameters since the CT band position is known to depend on both the length of Eu–O bond and the coordination environment around Eu^{3+} ions [22,23]. In this work, the CT band position variation is directly proportional to the Eu–O bond length, which increased with increasing temperatures. The La^{3+} in the as-synthesized monoclinic $LaPO_4$:Eu^{3+} was found to be nine-coordination with an average La–O bond length of 0.2611 nm, compared to the eight-coordination with an average La–O bond length of 0.2497 nm for the La^{3+} in the hexagonal $LaPO_4$:Eu^{3+} [21]. These factors made the average Eu–O bond length in the monoclinic $LaPO_4$:Eu^{3+} increased with increasing temperatures, and hence the red-shifted CT band.

Fig. 6(b) shows emission spectra for the resultant monoclinic $LaPO_4$:Eu^{3+}. Peaks at 585, 591, 612, 619, 650, 683, and 694 nm are assigned to the direct transition of $^5D_0$–$^7F_1$, $^5D_0$–$^7F_1$, $^5D_0$–$^7F_2$, $^5D_0$–$^7F_2$, $^5D_0$–$^7F_3$, $^5D_0$–$^7F_4$, $^5D_0$–$^7F_4$, respectively. The magnetic-dipole transition $^5D_0$–$^7F_1$ (585, 591 nm) was found to give the most pronounced emission from Eu^{3+} ions, leading to the orange-red light emitted by resulting materials. The emission from higher energy levels of Eu^{3+} ions ($^5D_1$, $^5D_2$) was difficult to be detected since the multiphoton relaxation based on the vibration of phosphate groups (ca.1067 cm^{-1}) effectively bridged gaps between the higher energy levels ($^5D_1$, $^5D_2$) and the lowest $^5D_0$ level of Eu^{3+} ions. The intensity of transitions between different J-number levels depends on the symmetry of the local environment of Eu^{3+} ions according to Judd–Ofelt theory [24–26]. In the present work, we found that the peak intensity for emissions associated with the $^5D_0$–$^7F_1$ transition increased with increasing annealing temperatures, which could be attributed to optimization of the crystal structure and gradually changes of the phase structure of resulting microspheres. A little increase of the luminescent intensity was observed when the annealing temperature increased from 800 °C to 900 °C. We also observed that the peak position at 589 nm in the hexagonal phase formed at 90 °C shifted to 593 nm in the monoclinic phase of the $LaPO_4$:Eu^{3+} formed at higher than 800 °C. This could be due to different lattice structures in the two phases of $LaPO_4$, which strongly depended on the orientation of the crystal axis relative to the polarization vector of the incident light [27].

Fig. 6(c) reproduces decay curves for the $^5D_0$–$^7F_1$ (λ = 591 nm) emission of Eu^{3+} ions in $LaPO_4$:Eu^{3+} microspheres prepared at different temperatures. Decay curves of Eu^{3+} ions were well fitted to the single-exponential function: $I = I_0 \exp(-t/t)$ (where t is the 1/e lifetime of Eu^{3+} ions). The lifetime of Eu^{3+} ions was calculated to be 1.726, 3.044, 3.062, 4.167 and 4.476 and 4.493 ms for $LaPO_4$:Eu^{3+} microspheres prepared at 90 °C, 500 °C, 600 °C, 700 °C 800 °C and 900 °C, respectively. The lifetime increased gradually with increasing annealing temperatures. The increase in rate became less significant over 800 °C due to the gradually changed phase structure of products and their perfect crystal structures.

For comparison, $LaPO_4$:Eu^{3+} bulk material was also prepared as reported elsewhere [14]. The XRD pattern of the bulk material indicates that it has the same phase structure as the as-prepared microspheres (Fig. S2, Supplementary materials). Fig. 7 shows luminescent properties of $LaPO_4$:Eu^{3+} microspheres annealed at

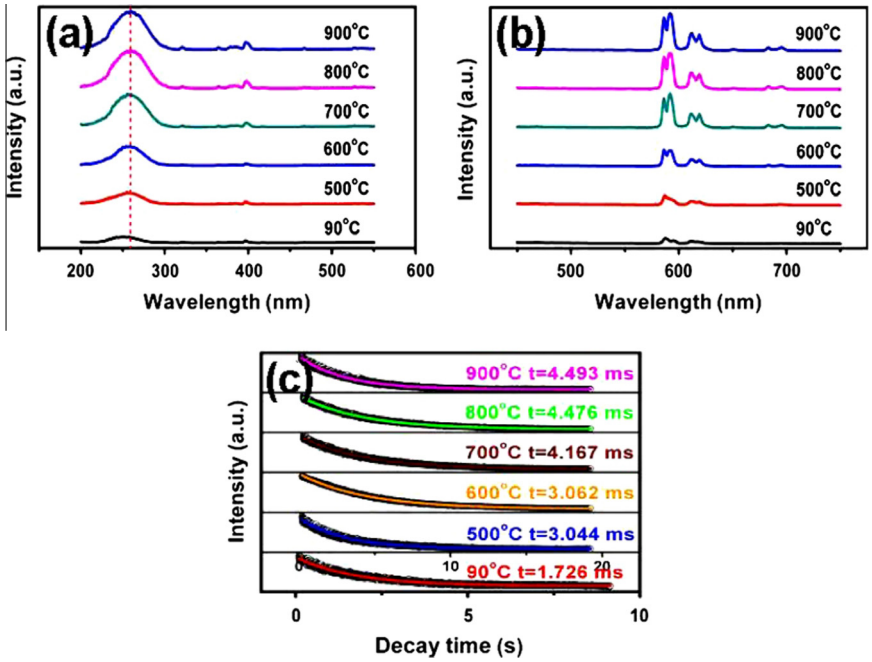

Fig. 6. (a) Excitation spectra, (b) emission spectra, and (c) decay curves for the $^5D_0$-$^7F_1$ (λ = 591 nm) emission of Eu^{3+} ions in $LaPO_4$:Eu^{3+} microspheres prepared at 90 °C for 10 h, followed by annealing at different temperatures for 2 h. Round circles represent experimental data. The solid lines are fitting results from $I(t) = A\exp(-t/\tau)$.

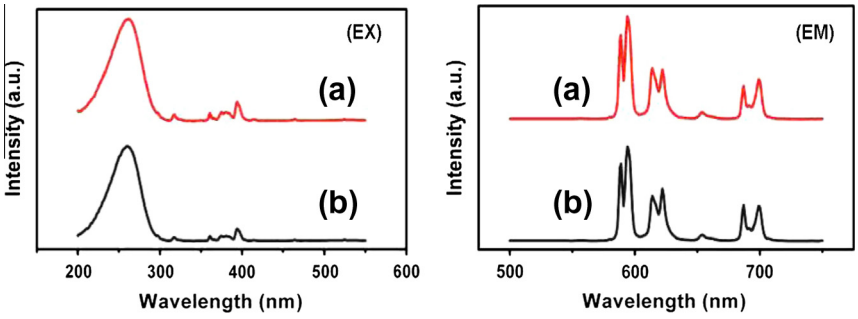

Fig. 7. Excitation (EX) and emission (EM) spectra of (a) $LaPO_4$:Eu^{3+} microspheres annealed at 800 °C, and (b) the $LaPO_4$:Eu^{3+} bulk material.

800 °C with respect to the as-synthesized bulk material. Under same experimental conditions (slits: 2.5, 2.5), the relative maximum intensity of $LaPO_4$:Eu^{3+} microspheres (0.54 g) is 2707 (wavelength: 594 nm), which is higher than that for the same amount of the bulk material (2169). This indicates that the special morphology of microscaled spheres enhance luminescent properties. However, both microspheres and the bulk material exhibited an almost difference in excitation and emission spectra. We further measured quantum efficiencies for microspheres and the bulk material. The quantum efficiency of microspheres (0.395) was found to be similar to that of the bulk material (0.406), suggesting that $LaPO_4$:Eu^{3+} microspheres could be utilized for applications where bulk materials were employed. While applications of $LaPO_4$:Eu^{3+} bulk materials are well-known to be largely limited by their non-uniform sizes (Fig. S3, Supplementary materials), $LaPO_4$:Eu^{3+} microspheres with a rather uniform size prepared in this work can be considered as potential alternatives to bulk materials.

4. Conclusions

We have presented a facile, but effective, two-step method for the preparation of monoclinic $LaPO_4$:Eu^{3+} microspheres. XRD patterns confirmed a pure monoclinic phase for resulting materials. SEM images revealed that $LaPO_4$:Eu^{3+} microspheres were composed of densely packed microprisms. Luminescent property measurements on the $LaPO_4$:Eu^{3+} microspheres prepared at 800 °C showed a higher luminescent intensity than that of primary hexagonal $LaPO_4$ microspheres. The luminescent intensity of $LaPO_4$:Eu^{3+} microspheres was found to be higher than that of corresponding bulk materials under identical conditions. Furthermore, microspheres possessed a more uniform morphology which could make better use of the exciting light source and reach a higher efficiency of the phosphor. As-synthesized monoclinic $LaPO_4$:Eu^{3+} microspheres have the potential to be used in various applications where bulk materials are employed. Therefore, the two-step approach developed in this work should provide effective pathways for circumventing the poor processibility intrinsically associated with bulk materials.

Acknowledgements

Financial supports from the Chinese National Nature Science Foundation (81000663), the Wenzhou Technological Project (S20130001), the Ministry of Education of China (211069, 20103321120003, IRT1077, SRF for ROCS), the Ministry of Science

and Technology of China (2009DFB30380), the National "Thousand Talents Program", the Zhejiang National Nature Science Foundation (Y13H180013), the Zhejiang Department of Education (T200917) and the Scientific development Foundation (KYQD120205) of Wenzhou Medical University are acknowledged.

Appendix A. Supplementary material

Supplementary data associated with this article can be found, in the online version, at http://dx.doi.org/10.1016/j.jallcom.2013.08.091.

References

[1] A.I. Becerro, S. Rodríguez-Liviano, A.J. Fernández-Carrión, M. Ocaña, Cryst. Growth Des. 13 (2013) 526–535.
[2] G.F. Ju, Y.H. Hu, L. Chen, X.J. Wang, Z.F. Mu, H.Y. Wu, F.W. Kang, J. Alloys Comp. 509 (2011) 5655–5659.
[3] K. Park, M.H. Heo, J. Alloys Comp. 509 (2011) 9111–9115.
[4] Y.P. Fang, A.W. Xu, R.Q. Song, H.X. Zhang, L.P. You, C. Jimmy, H.Q. Liu, J. Am. Chem. Soc. 125 (2003) 16025–16034.
[5] S. H Lee, K. Teshima, S. Mori, M. Endo, S.J. Oishi, Cryst. Growth Des. 10 (2010) 1693–1698.
[6] M.F. Dumont, C. Baligand, Y.C. Li, E.S. Knowles, M.W. Meisel, G.A. Walter, D.R. Talham, Bioconjugate Chem. 23 (2012) 951–957.
[7] G.Z. Chen, H.G. Zhao, F. Rosei, D.L. Ma, J. Phys. Chem. C 117 (2013) 10031–10038.
[8] Q. Zhang, T.P. Chou, B. Russo, S.A. Jenekhe, G. Cao, Angew. Chem. Int. Ed. 47 (2008) 2402–2406.
[9] N. Niu, P.P. Yang, Y. Wang, W.X. Wang, F. He, S.L. Gai, D. Wang, J. Alloys Comp. 509 (2011) 3096–3102.
[10] H. Wang, G.S. Li, X.F. Guan, L.P. Li, J. Alloys Comp. 509 (2011) 4160–4166.
[11] M. Yang, H.P. You, K. Liu, Y.H. Zheng, N. Guo, H.J. Zhang, Inorg. Chem. 49 (2010) 4996–5002.
[12] H. Wang, M. Miyauchi, Y. Ishikawa, A. Pyatenko, N. Koshizaki, Y. Li, L. Li, X. Li, Y. Bando, D. Golberg, J. Am. Chem. Soc. 133 (2011) 19102–19109.
[13] J. Huang, Y.H. Song, G.W. Wang, Y. Sheng, K.Y. Zheng, H.B. Li, H.G. Zhang, Q.S. Huo, X.C. Xu, H.F. Zou, J. Alloys Comp. 574 (2013) 310–315.
[14] N. Hashimoto, Y. Takada, K. Sato, S. Ibuki, J. Lumin. 48&49 (1991) 893–897.
[15] Y. Li, Y.D. Li, Z.X. Deng, J. Zhuang, X.M. Sun, Int. J. Inorg. Mater. 3 (2001) 633–637.
[16] X.M. Sun, X. Chen, Z.X. Deng, Y.D. Li, Mater. Chem. Phys. 78 (2002) 99.
[17] R.X. Yan, X.M. Sun, X. Wang, Q. Peng, Y.D. Li, Chem. Eur. J. 11 (2005) 2183–2195.
[18] S.P. Garcia, S. Semancik, Chem. Mater. 19 (2007) 4016–4022.
[19] D.S. Kilin, O.V. Prezhdo, Y.N. Xia, Chem. Phys. Lett. 58 (2008) 113–116.
[20] L. Li, W.G. Jiang, H.H. Pan, X.R. Xu, Y.X. Tang, J.Z. Ming, Z.D. Xu, R.K. Tang, Phys. Chem. C 111 (2007) 4111–4115.
[21] M. Yang, H.P. You, G. Jia, Y.J. Huang, Y.H. Song, Y.H. Zheng, K. Liu, Lihui Zhang, J. Cryst. Growth 311 (2009) 4753–4758.
[22] Y. Tao, G. Zhao, J. X. u, X. Shao, W. Zhang, S. Xia, Mater. Lett. 28 (1996) 137–140.
[23] Z. Wei, L. Sun, C. Liao, J. Yin, X. Jiang, C. Yan, J. Phys. Chem. B. 106 (2002) 10610–10617.
[24] B.R. Judd, Phys. Rev. 127 (1962) 750–761.
[25] G.S. Ofelt, J. Chem. phys. 37 (1962) 511–520.
[26] L.X. Yu, H.W. Son, S.Z. Lu, Z.X. Liu, L.M. Yang, X.G. Kong, J. Phys. Chem. B 108 (2004) 16697–16702.
[27] H. Meyssamy, K. Riwotzki, A. Kornowski, S. Naused, M. Haase, Adv. Mater. 11 (1999) 840–844.